Journal of Biomolecular NMR (2005) 33: 25–41
DOI 10.1007/s10858-005-2614-2


*Article*

# Comparison of $^{13}CH_3$, $^{13}CH_2D$, and $^{13}CHD_2$ methyl labeling strategies in proteins

Jason E. Ollerenshaw[a], Vitali Tugarinov[a,b,c], Nikolai R. Skrynnikov[d] & Lewis E. Kay[a,b,c,*]

[a]*Department of Chemistry, University of Toronto, Toronto, Ont., M5S 3H6, Canada;* [b]*Department of Biochemistry, University of Toronto, Toronto, Ont., M5S 1A8, Canada;* [c]*Department of Medical Genetics and Microbiology, University of Toronto, Toronto, Ont., M5S 1A8, Canada;* [d]*Department of Chemistry, Purdue University, West Lafayette, IN, 47907-2048, U.S.A.*

Received 29 April 2005; Accepted 25 July 2005

*Key words:* methyl groups, transverse relaxation optimized spectroscopy, isotopic labeling, malate synthase G, high molecular weight proteins

**Abstract**

A comparison of three labeling strategies for studies involving side chain methyl groups in high molecular weight proteins, using $^{13}CH_3$,$^{13}CH_2D$, and $^{13}CHD_2$ methyl isotopomers, is presented. For each labeling scheme, $^1H$–$^{13}C$ pulse sequences that give optimal resolution and sensitivity are identified. Three highly deuterated samples of a 723 residue enzyme, malate synthase G, with $^{13}CH_3$,$^{13}CH_2D$, and $^{13}CHD_2$ labeling in Ile δ1 positions, are used to test the pulse sequences experimentally, and a rationalization of each sequence's performance based on a product operator formalism that focuses on individual transitions is presented. The HMQC pulse sequence has previously been identified as a transverse relaxation optimized experiment for $^{13}CH_3$-labeled methyl groups attached to macromolecules, and a zero-quantum correlation pulse scheme ($^{13}CH_3$ HZQC) has been developed to further improve resolution in the indirectly detected dimension. We present a modified version of the $^{13}CH_3$ HZQC sequence that provides improved sensitivity by using the steady-state magnetization of both $^{13}C$ and $^1H$ spins. The HSQC and HMQC spectra of $^{13}CH_2D$-labeled methyl groups in malate synthase G are very poorly resolved, but we present a new pulse sequence, $^{13}CH_2D$ TROSY, that exploits cross-correlation effects to record $^1H$–$^{13}C$ correlation maps with dramatically reduced linewidths in both dimensions. Well-resolved spectra of $^{13}CHD_2$-labeled methyl groups can be recorded with HSQC or HMQC; a new $^{13}CHD_2$ HZQC sequence is described that provides improved resolution with no loss in sensitivity in the applications considered here. When spectra recorded on samples prepared with the three isotopomers are compared, it is clear that the $^{13}CH_3$ labeling strategy is the most beneficial from the perspective of sensitivity (gains ≥2.4 relative to either $^{13}CH_2D$ or $^{13}CHD_2$ labeling), although excellent resolution can be obtained with any of the isotopomers using the pulse sequences presented here.

## Introduction

Side chain methyl groups are emerging as valuable probes in NMR studies of the structure and dynamics of proteins (Muhandiram et al., 1995; Tugarinov et al., 2004a, 2005a). Their spectroscopic properties are favorable: methyl resonances are typically well-dispersed in $^1H$–$^{13}C$ correlation maps, and cross-correlations among the $^1H$–$^{13}C$ and $^1H$–$^1H$ dipolar interactions that mediate a methyl group's relaxation can be exploited to

*To whom correspondence should be addressed. E-mail: kay@pound.med.utoronto.ca

produce spectra with dramatically enhanced resolution (Ollerenshaw et al., 2003; Tugarinov et al., 2003). It is straightforward to produce protein samples that are $^{1}H,^{13}C$ labeled in selected side chain methyl positions and otherwise uniformly $^{2}H,^{12}C$ (Goto et al., 1999; Tugarinov et al., 2004a). This labeling strategy significantly decreases the relaxation rates of methyl coherences and allows the use of simple pulse sequences that target isolated $^{13}CH_3$ spin systems. Measurements of methyl–methyl distances via the nuclear Overhauser effect deliver a wealth of structural information on a protein's hydrophobic core regions (Metzler et al., 1996; Rosen et al., 1996; Smith et al., 1996; Gardner et al., 1997), where methyl groups tend to be concentrated (Janin et al., 1988). Millisecond dynamic processes can be measured at methyl positions using recently developed experiments (Ishima et al., 1999; Korzhnev et al., 2004), and accurate side chain order parameters can be derived from measurements of intra-methyl $^{1}H–^{13}C/^{1}H–^{1}H$ cross-correlation rates in small proteins (Tugarinov and Kay, 2004a) or through $^{2}H$ spin relaxation studies (Muhandiram et al., 1995; Millet et al., 2002).

Structural studies to date have concentrated on proteins labeled with $^{13}CH_3$ methyl groups at Ile ($\delta1$), Leu and Val residues, but it is also possible to prepare samples that are uniformly labeled at the same positions with either $^{13}CH_2D$ or $^{13}CHD_2$ isotopomers. This raises an interesting question: *Which of the three labeling patterns* ($^{13}CH_3$, $^{13}CH_2D$ or $^{13}CHD_2$) *is most advantageous with respect to signal-to-noise and resolution?* For example, reducing the number of $^{1}H$ spins in a methyl group attached to a protein may lead to a reduction of transverse relaxation rates due to the elimination of strong intra-methyl dipolar interactions. However, removing $^{1}H$ spins could also be detrimental because they will no longer contribute their steady-state polarization to the NMR signal, and the spin-lattice relaxation time of the remaining $^{1}H$ spins will be substantially increased. In order to address this question we first study a number of $^{1}H–^{13}C$ correlation pulse sequences and identify those which provide the best resolution and sensitivity for each isotopomer. Pulse sequences are tested experimentally using three samples of a 723 residue enzyme, malate synthase G (MSG), with $^{13}CH_3$, $^{13}CH_2D$, and $^{13}CHD_2$ labeling in Ile $\delta1$ positions. Subsequently a theoretical rationalization of each sequence's performance is presented, followed by a comparison of spectra recorded using the most favorable experiment in each case.

As has previously been reported, optimal spectra can be recorded for the $^{13}CH_3$ isotopomer using the HMQC pulse scheme (Ollerenshaw et al., 2003; Tugarinov et al., 2003) or using a zero-quantum correlation technique, $^{13}CH_3$ HZQC (Tugarinov et al., 2004b). We present a modified $^{13}CH_3$ HZQC sequence that boosts sensitivity by using steady-state $^{13}C$ magnetization in addition to polarization from protons. HSQC and HMQC spectra recorded on $^{13}CH_2D$ labeled Ile $\delta1$ methyls in MSG are of remarkably poor resolution. We demonstrate that, in the case of HSQC correlation maps, this is due to a $^{1}H–^{13}C$ dipolar cross-correlation effect, and we present a new transverse-relaxation optimized pulse sequence, $^{13}CH_2D$ TROSY, that exploits both $^{1}H–^{13}C$ and $^{1}H–^{1}H/^{1}H–^{13}C$ dipolar cross-correlations to record $^{1}H–^{13}C$ correlation spectra with greatly improved resolution in both $^{13}C$ and $^{1}H$ dimensions. For the $^{13}CHD_2$ isotopomer, spectra generated using HSQC and HMQC pulse schemes are of acceptable resolution and sensitivity; a $^{13}CHD_2$ HZQC experiment is described that takes advantage of intra-methyl $^{1}H–^{2}H/^{2}H–^{13}C$ dipolar cross-correlations to provide datasets with increased resolution.

The results strongly favor the use of $^{13}CH_3$ labeling at side chain methyl positions in structural studies of large proteins. While excellent resolution can be obtained in spectra of MSG recorded with any of the three isotopomers using the pulse sequences presented here, $^{1}H–^{13}C$ correlation maps of $^{13}CH_3$ methyl groups can be recorded with at least 2.4 times more sensitivity than is possible with either $^{13}CH_2D$ or $^{13}CHD_2$ methyls. These other isotopomers are, nonetheless, of considerable interest because of their use in studies of side chain dynamics through deuterium (Muhandiram et al., 1995; Tugarinov et al., 2005b) or carbon (Ishima et al., 1999, 2001) spin relaxation measurements.

## Materials and methods

### *NMR samples*

Three samples of MSG with different isotope labeling at Ile $\delta1$ positions were used in the present study, including U-[$^{15}N,^{2}H$], Ile $\delta1$-[$^{13}CH_3$]-labeled

MSG, U-[$^{15}$N,$^{2}$H], Ile δ1-[$^{13}CH_2D$]-labeled MSG, and U-[$^{15}$N,$^{2}$H], Ile δ1-[$^{13}CHD_2$]-labeled MSG. Each sample was prepared as described in detail previously (Tugarinov and Kay, 2004b) by *E. coli* overexpression in 1 litre of $D_2O$ M9 medium using U-[$^{2}$H]-glucose (CIL, Andover, MA) as the main carbon source and $^{15}NH_4Cl$ (CIL, Andover, MA) as the nitrogen source. One hour prior to induction, 100 mg of 4-$^{13}$C-3,3-$^{2}H_2$-α-ketobutyrate (Ile δ1-[$^{13}CH_3$] labeling), 4-$^{13}$C-3,3,4-$^{2}H_3$-α-ketobutyrate (Ile δ1-[$^{13}CH_2D$]-labeling), or 4-$^{13}$C-3,3,4,4-$^{2}H_4$-α-ketobutyrate (Ile δ1-[$^{13}CHD_2$] labeling) was added to the growth media. These α-ketobutyrate isotopomers were prepared from sodium 4-$^{13}$C-α-ketobutyrate, sodium 4-$^{13}$C-4-$^{2}$H-α-ketobutyrate, and sodium 4-$^{13}$C-4,4-$^{2}H_2$-α-ketobutyrate obtained from Isotec (Miamisburg, OH); the procedure of Gardner and Kay (1997) was used to deuterate the $C_3$ positions. Each of the three NMR samples was adjusted to have a protein concentration of $0.80 \pm 0.05$ mM and a pH of 7.1 (uncorrected), and contained 99.9% $D_2O$, 25 mM sodium phosphate, 20 mM $MgCl_2$, 0.05% $NaN_3$ and 5 mM DTT.

*NMR spectroscopy*

All NMR experiments were performed at 37 °C on a 500 MHz Varian Unity Inova spectrometer equipped with a room temperature pulsed field gradient triple resonance probe. Datasets were obtained with (100, 512) complex points in the ($^{13}$C, $^{1}$H) dimensions, corresponding to acquisition times of (80, 64 ms), with the exception of the HSQC and HMQC datasets recorded on the Ile δ1-[$^{13}CH_2D$]-labeled sample, which comprised (40, 512) complex points corresponding to acquisition times of (32, 64 ms). A relaxation delay of 1.5 s was used for each experiment (excepting the non-sensitivity-enhanced HSQC spectrum of the Ile δ1-[$^{13}CH_2D$]-labeled sample used to prepare Figure 7a, for which 1.2 s was used; intensities were subsequently corrected for the reduced relaxation delay using independently measured $T_1$ values so that in all comparisons of datasets the same effective delay, 1.5 s, was employed) and 16 scans/FID were recorded (40 scans/FID for the HSQC and HMQC spectra of the Ile δ1-[$^{13}CH_2D$]-labeled sample), for total measurement times of 90 min per experiment.

All NMR spectra were processed using the NMRPipe/NMRDraw suite of programs (Delaglio et al., 1995). The relaxation rates listed in Table 1 were measured using straightforward modifications of the pulse schemes described in the text. $R_1$ and $R_2$ rates were extracted separately for each residue by least-squares fitting experimental decay curves to the exponential function $I(T) = A\exp(-RT)$, where $T$ is a parametric relaxation delay.

## Results and discussion

As described briefly in Materials and methods and in detail in a series of previous publications (Gardner and Kay, 1997; Goto et al., 1999; Tugarinov and Kay, 2004b) it is possible to prepare highly deuterated protein, with protonation restricted to Ile (δ1), Leu and Val methyl positions. With the recent introduction of commercially available ketobutyrates/isovalerates with $^{13}CH_2D$ and $^{13}CHD_2$ labeling, in addition to the more common $^{13}CH_3$-based precursors, it is now possible to generate samples that are uniform in the isotopomer of choice. Three samples of MSG that are $^{13}CH_3$,$^{13}CH_2D$, or $^{13}CHD_2$ labeled at Ile δ1 positions and are otherwise highly deuterated and as similar as possible have been produced and their $^{1}$H–$^{13}$C correlation spectra are overlaid in Figure 1. The isotopomers of a given Ile δ1 methyl group can be distinguished by their slightly different $^{13}$C and $^{1}$H chemical shifts (due to $^{2}$H isotope shifts of $\sim -0.3$ and $\sim -0.02$ ppm per deuteron, respectively). It is worth emphasizing that only a single isotopomer is observed in spectra of each sample, with the exception of $CH_2D$ labeled MSG that is ~10% contaminated with the $^{13}CHD_2$ isotopomer due to a 10% 4-$^{13}$C-4,4-$^{2}H_2$-α-ketobutyrate impurity in the purchased 4-$^{13}$C-4-$^{2}$H-α-ketobutyrate starting material.

*TROSY $^{1}H$–$^{13}C$ correlation experiments for macromolecular $^{13}CH_nD_{3-n}$ methyl groups*

The development of TROSY spectroscopy (Pervushin et al., 1997) has significantly increased the size of biomolecules that are amenable to study by solution NMR techniques. TROSY-based experiments take advantage of cross-correlated relaxation interactions to increase both spectral resolution and sensitivity. Cross-correlation effects, resulting from interference between the different magnetic interactions that mediate the decoherence of a spin system, can divide coherence into two

classes: one that is fast-relaxing due to constructive interference between the cross-correlated interactions, and a second that is slowly-relaxing due to destructive interference. TROSY pulse sequences exploit this separation by creating coherence transfer pathways that involve only slowly-relaxing coherences. This reduces the relaxation rate during indirect chemical shift encoding steps and during acquisition, ensuring optimal resolution while maximizing peak heights, and relaxation losses during transfer steps are minimized for optimal sensitivity. In contrast, non-TROSY experiments tend to interconvert slowly- and fast-relaxing coherences during decoupling steps and heteronuclear transfers so that there is less benefit from the existence of the slowly-relaxing coherences.

### *$^{13}CH_3$ methyl groups*

It has already been established that HMQC (Müller, 1979; Bax et al., 1983) is a TROSY $^{1}H$–$^{13}C$ correlation experiment for $^{13}CH_3$ methyl groups in large proteins (Ollerenshaw et al., 2003; Tugarinov et al., 2003). In the case of an isolated $^{13}CH_3$ spin system that is attached to a slowly tumbling molecule but that itself rotates rapidly about its symmetry axis, cross-correlations between different $^{1}H$–$^{1}H$ dipolar interactions give rise to distinct slowly- and fast-relaxing $^{1}H$ single-quantum coherences (Werbelow and Marshall, 1973; Kay and Prestegard, 1987; Muller et al., 1987). In a similar manner, interference between $^{1}H$–$^{1}H$ dipolar interactions and between $^{1}H$–$^{13}C$ dipolar interactions establish slowly- and fast-relaxing $^{1}H$–$^{13}C$ multiple-quantum coherences (Tugarinov et al., 2003). While the fast-relaxing coherences decay too rapidly to be useful, relaxation rates for the slowly-relaxing coherences are very favorable, as shown by the experimentally measured values for MSG listed in Table 1. The HMQC experiment provides optimal resolution and sensitivity because slowly-relaxing $^{1}H$ single-quantum coherence created by the sequence's initial pulse is converted to slowly-relaxing $^{1}H$–$^{13}C$ multiple-quantum coherence for $^{13}C$ chemical shift encoding and then back to slowly-relaxing $^{1}H$ single-quantum coherence for detection. Other correlation experiments such as HSQC (Bodenhausen and Rubin, 1980) contain additional $\pi/2$ $^{1}H$ pulses that spoil the TROSY enhancement by mixing slowly- and fast-relaxing coherences, and therefore perform poorly compared to HMQC. For example, peaks in the HMQC spectrum of $^{13}CH_3$-labeled MSG at 37 °C (Figure 2aii) are on average more than twice as intense as the corresponding peaks in the HSQC spectrum (Figure 2ai).

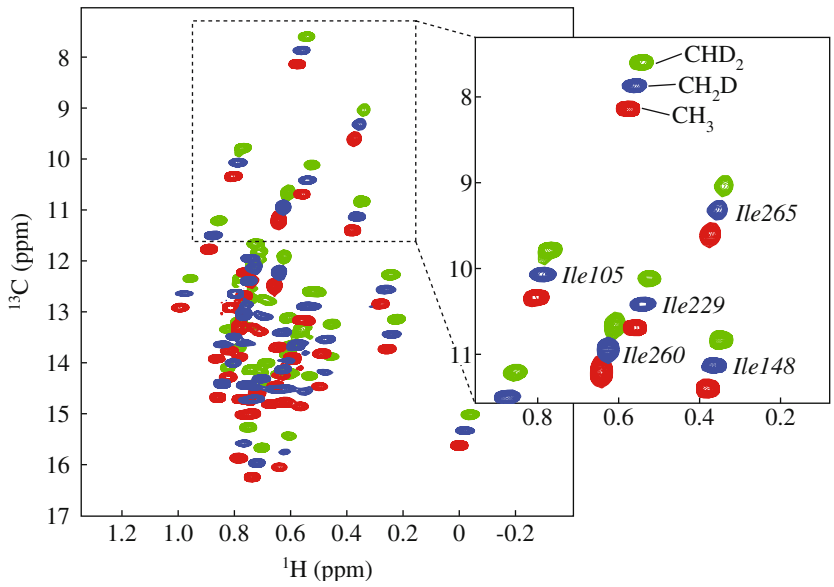


*Figure 1.* Overlaid $^{1}H$–$^{13}C$ correlation spectra from highly deuterated samples of malate synthase G with $^{13}CH_3$ (red), $^{13}CH_2D$ (blue) and $^{13}CHD_2$ (green) labeling at Ile δ1 positions. The HMQC pulse sequence was used to record the spectra of the $^{13}CH_3$ and $^{13}CHD_2$ samples, while the $^{13}CH_2D$ TROSY pulse sequence shown in Figure 5 was used for the $^{13}CH_2D$ sample. Signal intensities have been adjusted for clarity and do not reflect the relative signal-to-noise ratios of the individual spectra.

*Table 1.* Average experimental relaxation rates measured for $^{13}CH_3$, $^{13}CH_2D$, and $^{13}CHD_2$-labeled Ile δ1 methyl groups in malate synthase G[a]

| Isotopomer | $^1H$ $R_2(s^{-1})$ | | $^{13}C$ $R_2$ $(s^{-1})$ | | $^1H$ $R_1(s^{-1})$ | |
|---|---|---|---|---|---|---|
| $^{13}CH_3$[b] | $R_{2,H}^{s,CH_3}$ | $26.4 \pm 8.8$ | $R_{2,H}^{s,CH_3}$ | $21.7 \pm 12.1$ | $R_{1,H}^{CH_3}$ | $1.0 \pm 0.2$ |
| | $R_{2,H}^{f,CH_3}$ | 277[c] | $R_{2,CH}^{f,CH_3}$ | 311[c] | | |
| $^{13}CH_2D$[d] | $R_{2,H}^{s,CH_2D}$ | $33.5 \pm 12.1$ | $R_{2,C}^{s,CH_2D}$ | $13.8 \pm 11.6$[e] | $R_{1,H}^{CH_2D}$ | $0.8 \pm 0.2$ |
| | $R_{2,H}^{f,CH_2D}$ | $124.6 \pm 53.1$ | $R_{2,C}^{f,CH_2D}$ | $52.1 \pm 19.2$[e] | | |
| $^{13}CHD_2$ | $R_{2,H}^{CHD_2}$ | $23.0 \pm 6.5$ | $R_{2,C}^{f,CHD_2}$ | $23.0 \pm 10.0$[e] | $R_{1,H}^{CHD_2}$ | $0.4 \pm 0.1$ |

[a]Relaxation measurements were made using a 500 MHz spectrometer with samples of MSG dissolved in $D_2O$ at 37°C (see Materials and methods). Rates reported for the $^{13}CH_3$, $^{13}CH_2D$, and $^{13}CHD_2$ isotopomers are averaged over 38, 29, and 34 of the 44 Ile δ1 methyl groups in MSG, respectively.
[b]For the $^{13}CH_3$ isotopomer, rates are given for slowly- and fast-relaxing forms of both $^1H$ single quantum and $^1H$–$^{13}C$ multiple quantum coherence, as defined by Ollerenshaw et al. (2003).
[c]Theoretical estimate.
[d]The transverse relaxation rates given for the $^{13}CH_2D$ isotopomer correspond to those defined in Figure 4.
[e]Measured in the presence of $^2H$ decoupling.

A $^1H$–$^{13}C$ zero-quantum correlation experiment for $^{13}CH_3$ groups in large proteins, $^{13}CH_3$ HZQC, that offers a substantial resolution enhancement in $F_1$ over HMQC has also been described (Tugarinov et al., 2004b). The experiment relies on the fact that $^1H$–$^{13}C$ heteronuclear zero-quantum coherences relax less rapidly than the corresponding double-quantum elements due to cross-correlation effects involving dipolar interactions between the methyl $^1H$, $^{13}C$ spins and proximal spins (either protons or deuterons). The HMQC pulse sequence interconverts heteronuclear double- and zero-quantum coherences halfway through $t_1$, but in the $^{13}CH_3$ HZQC scheme this interconversion is avoided and relaxation during $t_1$ proceeds at the slow zero-quantum rate, resulting in reduced linewidth in the indirectly detected dimension. This resolution enhancement comes at the expense of sensitivity because half of the initial magnetization is lost to a coherence transfer pathway involving double-quantum coherence during $t_1$, but this loss is mitigated by a sensitivity enhancement scheme in which both cosine- and sine-modulated $t_1$ components of the signal are preserved. (The same enhancement cannot be achieved in the HMQC experiment without spoiling the $^{13}CH_3$ TROSY effect.) To further improve sensitivity, we have modified the $^{13}CH_3$ HZQC pulse sequence to make use of steady-state $^{13}C$ magnetization in addition to $^1H$ magnetization (Figure 3). When applied to $^{13}CH_3$-labeled MSG, this experiment (Figure 2aiii) is 18% more sensitive than the previous HZQC experiment (Tugarinov et al., 2004b) (spectrum not shown; average over 43 residues). Importantly, the new $^{13}CH_3$ HZQC experiment is marginally more sensitive than HMQC (Figure 2aii) and produces a spectrum with noticeably improved linewidths in the indirectly detected dimension. The relative sensitivities of HSQC (Figure 2ai), HMQC (Figure 2aii) and HZQC (Figure 2aiii) datasets recorded on MSG at 37 °C ($\tau_c \sim 55$ ns at the concentrations used here) are 0.44:1.0:0.92, quantified from a set of 36 correlations that are well resolved in each of the datasets. Corresponding histograms of residue-specific intensities relative to the HMQC dataset are shown in Figure 2aiv,v.

### *$^{13}CH_2D$ methyl groups*

Recently Bax and coworkers have published a TROSY experiment for methylene $^{13}CH_2$ groups and demonstrated its utility for studies of both proteins and nucleic acids (Miclet et al., 2004). There are important relaxation differences between $^{13}CH_2$ spin systems that undergo rapid rotation, as in a $^{13}CH_2D$ methyl, and those that are essentially static, as in a methylene, so that a sequence optimized for one of these cases would be ineffective for the other. A comparison of the different classes of $^{13}CH_2$ spin system is beyond the scope of the present work; suffice it to say that the differences in large part arise from a sign inversion in $^1H$–$^{13}C$ cross-correlation derived terms so that fast-relaxing $^{13}C$ lines in one case become slowly-relaxing in the other.

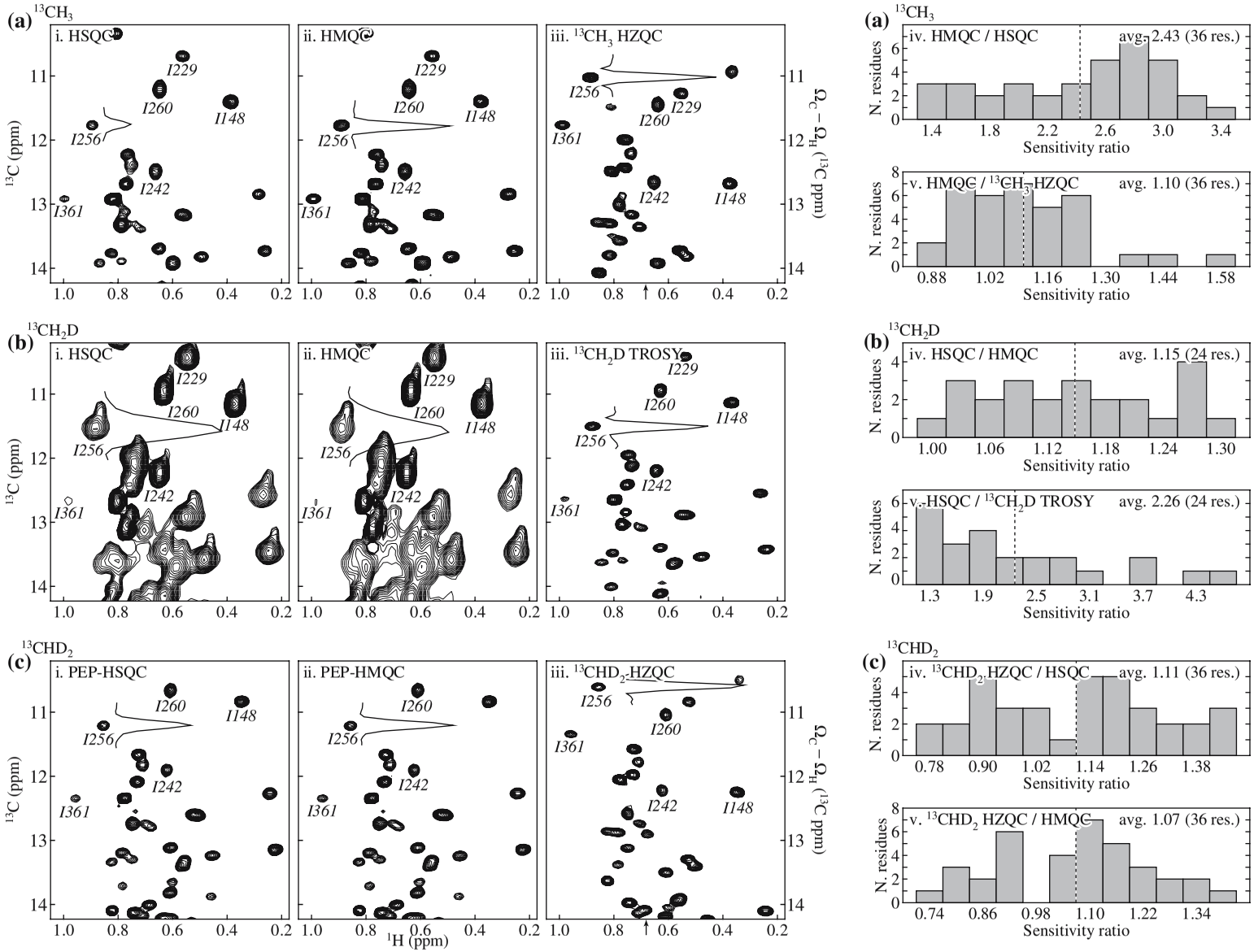
(a) $^{13}CH_3$
i. HSQC
ii. HMQC
iii. $^{13}CH_3$ HZQC
(b) $^{13}CH_2D$
i. HSQC
ii. HMQC
iii. $^{13}CH_2D$ TROSY
(c) $^{13}CHD_2$
i. PEP-HSQC
ii. PEP-HMQC
iii. $^{13}CHD_2$-HZQC
I229
I260
I148
I256
I242
I361
$^{13}C$ (ppm)
$^{1}H$ (ppm)
$\Omega_C - \Omega_H$ ($^{13}C$ ppm)
(a) $^{13}CH_3$
iv. HMQC / HSQC
avg. 2.43 (36 res.)
v. HMQC / $^{13}CH_3$-HZQC
avg. 1.10 (36 res.)
(b) $^{13}CH_2D$
iv. HSQC / HMQC
avg. 1.15 (24 res.)
v. HSQC / $^{13}CH_2D$ TROSY
avg. 2.26 (24 res.)
(c) $^{13}CHD_2$
iv. $^{13}CHD_2$-HZQC / HSQC
avg. 1.11 (36 res.)
v. $^{13}CHD_2$ HZQC / HMQC
avg. 1.07 (36 res.)
N. residues
Sensitivity ratio

*Figure 2.* $^{1}H$–$^{13}C$ correlation spectra of (a) $^{13}CH_3$, (b) $^{13}CH_2D$, and (c) $^{13}CHD_2$ Ile δ1-labeled samples of highly deuterated malate synthase G recorded as described in Materials and methods using (i) HSQC, (ii) HMQC, and (iii) relaxation-optimized pulse sequences, along with (iv, v) histograms of signal-to-noise ratios obtained from selected pairs of experiments. All spectra were scaled to have the same noise floor and are plotted at the same contour level so that peak intensities are directly comparable. To aid in comparison, assignments to Ile δ1 methyl groups are indicated for selected peaks, and a trace along the indirectly detected dimension through the peak corresponding to Ile 256 is superimposed on each spectrum. The spectra in (aiii), (biii), and (ciii) were recorded using the $^{13}CH_3$ HZQC, $^{13}CH_2D$ TROSY, and $^{13}CHD_2$ HZQC pulse sequences shown in Figures 3, 5, and 6, respectively. In the two HZQC spectra, correlations appear at frequencies of $(\Omega_C-\Omega_H)$ in the indirectly detected dimension, where $\Omega_C$ and $\Omega_H$ are the offsets from the $^{13}C$ and $^{1}H$ carriers, and the scale in this dimension is in units of ppm relative to the $^{13}C$ carrier; the $^{1}H$ carrier frequency is indicated by an arrow along the $^{1}H$ chemical shift axis. The spectra in (bi) and (bii) were recorded with a shorter $t_1$ acquisition time than for other spectra (32 vs. 80 ms; see Materials and methods) to compensate for rapid relaxation during $t_1$; in these experiments the number of scans/FID was increased to obtain the same measurement time as for the other spectra. The spectra in (ci) and (cii) were recorded using enhanced sensitivity pulsed field gradient versions of the HSQC and HMQC pulse sequences (Kay et al., 1992; Schleucher et al., 1993). The histograms were based on the quantification of 36, 24 and 36 correlations for $^{13}CH_3$, $^{13}CH_2D$, and $^{13}CHD_2$ spectra, respectively; the average sensitivity ratio is indicated by a dashed line in each plot.

The need to develop a TROSY $^{1}H$–$^{13}C$ correlation experiment for studies of $^{13}CH_2D$ groups attached to macromolecules becomes apparent upon inspection of both HSQC and HMQC spectra recorded on such spin systems, illustrated in Figure 2bi, ii, for Ile $^{13}CH_2D$ labeled MSG. To understand why such correlation maps are so poorly resolved, it is necessary to consider the relaxation properties of a $^{13}CH_2D$ methyl group tumbling in the macromolecular limit (defined as $\omega_C\tau_C \gg 1$, where $\omega_C$ is the $^{13}C$ resonance frequency and $\tau_C$ is the tumbling correlation time) in detail. Figure 4 shows the energy level diagram of a $^{13}CH_2$ spin system in a basis of eigenstates of the system's free precession Hamiltonian. The single-exponential relaxation rates indicated in Figure 4 for single-quantum $^{1}H$ and $^{13}C$ transitions are derived assuming that: (1) the methyl group has regular tetrahedral geometry and rotates rapidly about its symmetry axis, so that auto- and cross-correlation spectral densities for a pair of similar interactions are equal (Kay and Torchia, 1991); (2) $\omega_C\tau_C \gg 1$, so that only terms proportional to $\tau_C$ are important to transverse relaxation; (3) only intra-methyl $^{1}H$–$^{1}H$ and $^{1}H$–$^{13}C$ dipolar interactions contribute to relaxation.

Notably, contributions from the pair of $^{1}H$–$^{13}C$ dipolar interactions lead to slowly- and fast-relaxing $^{13}C$ single-quantum coherences. As a result of destructive interference, $^{13}C$ coherence associated with the $^{1}H$ state $|2\rangle$ is unaffected by $^{1}H$–$^{13}C$ dipolar interactions and relaxes at the slow rate $R_{2,C}^{s,CH_2D}$ given in Figure 4. ($^{13}C$ coherence associated with $^{1}H$ state $|4\rangle$ also relaxes slowly, but is of limited interest because it cannot be efficiently prepared from steady-state $^{1}H$ magnetization.) On the other hand, the relaxation of $^{13}C$ lines with $^{1}H$ spin states $|1\rangle$ or $|3\rangle$ is enhanced by constructive interference

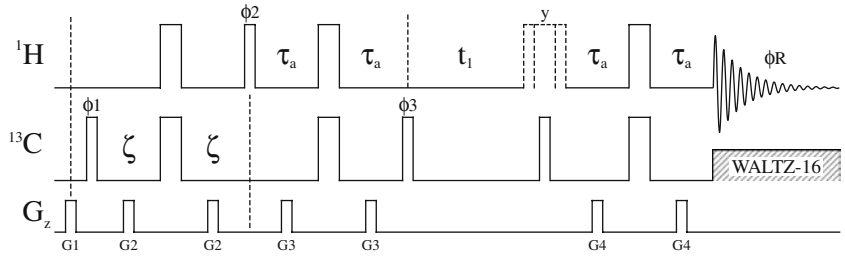


*Figure 3.* Improved pulse sequence for zero-quantum $^{1}H$–$^{13}C$ correlation spectroscopy of macromolecular $^{13}CH_3$-labeled methyl groups ($^{13}CH_3$ HZQC). Each narrow (wide) rectangular pulse is applied along the $x$-axis with the highest available power and with a tip angle of $\pi/2$ ($\pi$), unless otherwise indicated. During the $^{1}H$ acquisition period, $^{13}C$ WALTZ-16 decoupling (Shaka et al., 1983) is applied using a 2–3 kHz field. For each $t_1$ point, the pulse sequence is repeated with and without the composite $^{1}H$ π pulse drawn in dotted lines, giving rise to two separate datasets that are subsequently added and subtracted to generate sensitivity-enhanced hypercomplex data as described previously (Cavanagh and Rance, 1993 ). Pulse phases are cycled as follows: $\phi1 = -y, -x, y, x$; $\phi2 = x, y$; $\phi3 = y, x, -y, -x$; and $\phi R = x, x, -x, -x$. Delay $\zeta$ is set to 750 $\mu$s and $\tau_a$ is set to 1.8 ms. Field gradient pulses ($G_z$) are applied along the $z$-axis and have the following (durations, strengths): G1 = (2 ms, 4 G/cm), G2 = (0.3 ms, 24 G/cm), G3 = (0.5 ms, 15 G/cm), and G4 = (1 ms, −10 G/cm).

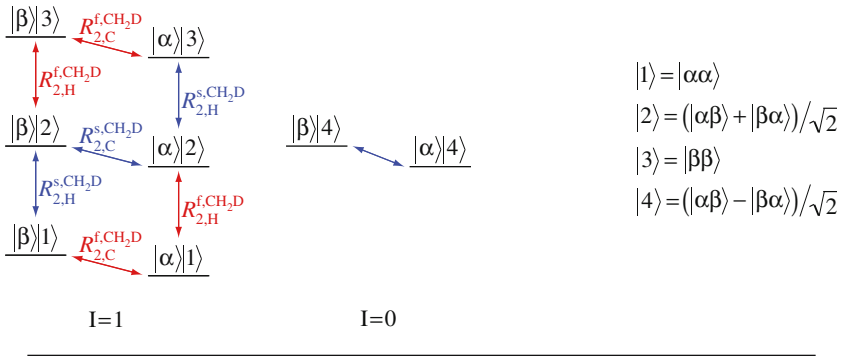


$$R_{2,C}^{f,CH_2D} = \frac{4}{45}\left(\frac{\mu_0}{4\pi}\right)^2 \frac{S_{axis}^2\gamma_H^2\gamma_C^2\hbar^2\tau_C}{r_{HC}^6} \qquad R_{2,C}^{s,CH_2D} = 0$$

$$R_{2,H}^{f,CH_2D} = \frac{9}{80}\left(\frac{\mu_0}{4\pi}\right)^2 \frac{S_{axis}^2\gamma_H^4\hbar^2\tau_C}{r_{HH}^6} + \frac{1}{45}\left(\frac{\mu_0}{4\pi}\right)^2 \frac{S_{axis}^2\gamma_H^2\gamma_C^2\hbar^2\tau_C}{r_{HC}^6} + \frac{1}{10}\left(\frac{\mu_0}{4\pi}\right)^2 \frac{S_{axis}^2\gamma_H^3\gamma_C\hbar^2\tau_C}{r_{HH}^3 r_{HC}^3}$$

$$R_{2,H}^{s,CH_2D} = \frac{9}{80}\left(\frac{\mu_0}{4\pi}\right)^2 \frac{S_{axis}^2\gamma_H^4\hbar^2\tau_C}{r_{HH}^6} + \frac{1}{45}\left(\frac{\mu_0}{4\pi}\right)^2 \frac{S_{axis}^2\gamma_H^2\gamma_C^2\hbar^2\tau_C}{r_{HC}^6} - \frac{1}{10}\left(\frac{\mu_0}{4\pi}\right)^2 \frac{S_{axis}^2\gamma_H^3\gamma_C\hbar^2\tau_C}{r_{HH}^3 r_{HC}^3}$$

*Figure 4*. Energy level diagram of a $^{13}CH_2$ spin system, with relaxation rate expressions for selected single-quantum $^1H$ and $^{13}C$ coherences. The rate expressions apply to an isolated $^{13}CH_2$ system tumbling in the macromolecular limit, subject to conditions given in the text. $S_{axis}$ is an order parameter describing the amplitude of motion of the methyl threefold axis, $\delta_i$ is the gyromagnetic ratio of spin $i$,$\tau_C$ is the (assumed isotropic) molecular tumbling time, and $r_{AB}$ is the distance between spins A and B in a $^{13}CH_2D$ methyl group.

and proceeds at the fast rate $R_{2,C}^{f,CH_2D}$. The magnitude of this cross-correlation effect is striking, with the average experimental values of $R_{2,C}^{s,CH_2D}$ and $R_{2,C}^{f,CH_2D}$ measured for Ile δ1 $^{13}CH_2D$ groups in MSG (Table 1) differing by nearly a factor of four, and is responsible for the HSQC experiment's poor performance when applied to $^{13}CH_2D$ methyl groups attached to large molecules.

It is straightforward to show that the initial INEPT transfer in the HSQC pulse scheme converts steady-state $^1H$ magnetization into exclusively fast-relaxing $^{13}C$ coherence. This coherence decays rapidly during the $^{13}C$ chemical shift encoding period, $t_1$, resulting in poor resolution in the $^{13}C$ dimension. The HMQC experiment, while not affected by $^1H$–$^{13}C$ cross-correlation, performs poorly because the multiple-quantum coherences present during $t_1$ are relaxed by both $^1H$–$^1H$ and $^1H$–$^{13}C$ dipolar interactions within the methyl and are subject to especially substantial relaxation contributions due to interactions with external spins. Interestingly, zero-quantum coherences relax much more slowly than double-quantum coherences due to cross-correlation between $^1H$–$^1H$ and $^1H$–$^{13}C$ intra-methyl dipolar interactions, but the theoretically predicted relaxation rate for zero-quantum coherence (29 $s^{-1}$ calculated for $\tau_c = 56$ ns, $S_{axis}^2 = 0.6$) is still more than double the average experimentally observed value of $R_{2,C}^{s,CH_2D}$ (Table 1). Clearly, in order to deliver optimal resolution, a TROSY experiment for macromolecular $^{13}CH_2D$ groups must use slowly-relaxing $^{13}C$ single-quantum coherence during $t_1$.

We have therefore developed a modified HSQC pulse sequence, $^{13}CH_2D$ TROSY, that uses a mixing element to transform fast-relaxing into slowly-relaxing $^{13}C$ coherence before the $^{13}C$ chemical shift encoding period (Figure 5). Like HSQC, the sequence starts with the transfer of steady-state $^1H$ magnetization to antiphase $^{13}C$ single-quantum coherence[1], $\rho = -2C_yH_z = -2C_y|1\rangle\langle 1| + 2C_y|3\rangle\langle 3|$ (point *a* in Figure 5), where $H_z = H_{1z} + H_{2z}$ and $H_{iz}$ is the *z*-magnetization of $^1H$ i. This fast-relaxing coherence is allowed to evolve under $^1H$–$^{13}C$ scalar coupling for a period of $\tau_b = 1/(4J_{CH})$ so that it becomes in-phase with respect to the $^1H$ spins, and a $\pi/2$ $C_y$

[1]In this notation the density matrix for a $^{13}CH_2D$ spin system is written as the tensor product of a $^{13}C$ spin operator and an operator representing the state of the two $^1H$ spins in the numbered basis defined in Figure 4. For example, $2C_x|2\rangle\langle 2| = C_x \otimes (|\alpha\beta\rangle + |\beta\alpha\rangle)(\langle\alpha\beta| + \langle\beta\alpha|)$ and $\sqrt{2}C_\beta|1\rangle\langle 2| = |\beta\rangle\langle\beta| \otimes |\alpha\alpha\rangle(\langle\alpha| + \langle\beta\alpha|)$.

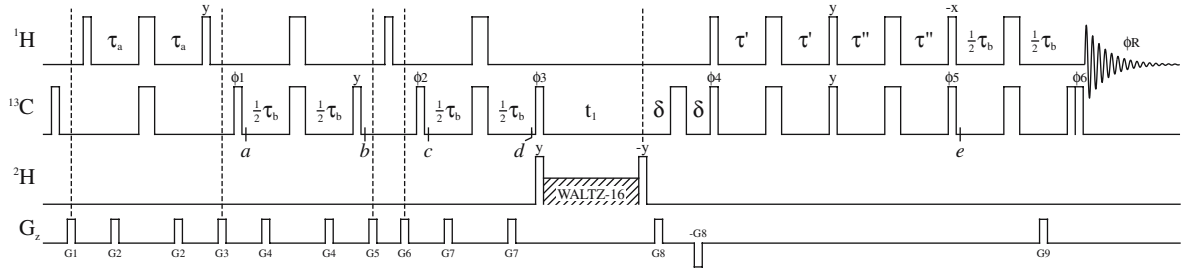


*Figure 5*. Relaxation-optimized pulse sequence for single-quantum $^1$H–$^{13}$C correlation spectroscopy of $^{13}CH_2D$-labeled methyl groups ($^{13}CH_2D$ TROSY). Each narrow (wide) rectangular pulse is applied along the *x*-axis with the highest available power (for $^1$H/$^{13}$C; 2 kHz for $^2$H) and with a tip angle of $\pi/2(\pi)$, unless otherwise indicated. During $t_{19}$ $^2$H WALTZ-16 decoupling (Shaka et al., 1983) is applied using a 0.75 kHz field. Pulse phases are cycled as follows: $\phi1 = x, -x$; $\phi2 = x, x, -x, -x$; $\phi3 = 4(y), 4(-y)$; $\phi4 = x$; $\phi5 = -x$; $\phi6 = -x$; and $\phi R = x, -x, -x, x$. The delays used are $\tau_a = 1.8$ ms, $\tau_b = 2.0$ ms, $\tau' = 0.667$ ms, and $\tau'' = 0.784$ ms. Field gradient pulses ($G_z$) are applied along the *z*-axis and have the following (durations, strengths): G1 = (1.0 ms, 15 G/cm), G2 = (0.5 ms, 20 G/cm), G3 = (1.0 ms, −16 G/cm), G4 = (0.15 ms, 4 G/cm), G5 = (0.5 ms, 24 G/cm), G6 = (0.25 ms, 24 G/cm), G7 = (0.3 ms, −10 G/cm), G8 = (0.25 ms, 60 G/cm), and G9 = (0.125 ms, 59.36 G/cm). Quadrature detection in the indirectly detected dimension is achieved via the enhanced sensitivity pulsed field gradient method (Kay et al., 1992; Schleucher et al., 1993), where for each value of $t_1$ separate datasets are recorded for (g9, $\phi4$) and (−g9, $-\phi4$). Splittings in the $^1$H dimension due to $^1$H–$^{13}$C scalar coupling are removed by recording separate datasets for each complex $t_1$ point for ($\phi5$, $\phi6$) and ($-\phi5$, $-\phi6$) and processing them as described in Appendix A.

pulse is applied to produce longitudinal $^{13}$C magnetization associated with the $^1$H states $|1\rangle$ and $|3\rangle$: $\rho = -2C_zH_z^2 = -(2C_z|1\rangle\langle1| + 2C_z|3\rangle\langle3|)$ (point *b*). The goal at this point is to optimally convert ρ into $C_z|2\rangle\langle2|$, since the relaxation of $C_{x,y}|2\rangle\langle2|$ is much less efficient than $C_{x,y}|1\rangle\langle1|$, $C_{x,y}|3\rangle\langle3|$ (Figure 4). This is accomplished through the application of a $^1$H $\pi/2$ pulse, which leaves the system in the state $\rho = -2C_z|2\rangle\langle2| + C_z|1\rangle\langle1| + C_z|3\rangle\langle3| - C_z|1\rangle\langle3| - C_z|3\rangle\langle1|$). Subsequently, application of gradient g6 dephases the double quantum terms, and a $\pi/2$ $^{13}$C pulse creates a mixture of fast- and slowly-relaxing $^{13}$C single-quantum coherences, $\rho = -(2C_y|2\rangle\langle2| + C_y|1\rangle\langle1| + C_y|3\rangle\langle3|$ (point *c*). Neglecting relaxation losses, $1/\sqrt{2}$ of the initial $^1$H magnetization has been transferred to slowly-relaxing $2C_y|2\rangle\langle2|$ at this point (see Appendix B). Next, the remaining fast-relaxing $^{13}$C coherence is filtered out by exploiting the fact that the slowly-relaxing coherence does not evolve under $^1$H–$^{13}$C scalar coupling. After a $J_{CH}$ evolution period of duration $\tau_b = 1/(4J_{CH})$ (between points *c* and *d*), $\rho = -2C_y|2\rangle\langle2| + C_x|1\rangle\langle1| - C_x|3\rangle\langle3|$, and the fast-relaxing component is then placed along the *z*-axis by a $^{13}$C pulse along *y* which is phase cycled ($\phi3$ in Figure 5) to ensure the affected magnetization makes no contribution to the final dataset. Finally, the isolated slowly-relaxing $^{13}$C single-quantum coherence is allowed to evolve in the presence of $^2$H decoupling during the $^{13}$C chemical shift encoding period, to produce $\rho = 2C_y|2\rangle\langle2|\cos(\Omega_C t_1) + 2C_x|2\rangle\langle2|\sin(\Omega_C t_1)$ where $\Omega_C$ is the offset frequency of the $^{13}$C spin.

The rest of the pulse sequence serves to transfer the slowly-relaxing $^{13}$C coherence back to protons for detection. It is possible to achieve this by reversing the coherence transfer pathway traversed in the first part of the experiment. Because such a scheme involves a second $^1$H mixing pulse (efficiency $1/\sqrt{2}$), the net sensitivity, neglecting relaxation, is half that of a regular HSQC. In applications to large proteins, where relaxation effects cannot be neglected, some of the intrinsic sensitivity loss can be compensated for by the improved relaxation characteristics during $t_1$; in applications involving MSG, datasets with dramatically improved resolution in the $^{13}$C dimension relative to HSQC maps are obtained (data not shown). However, we present below a more optimal method to transfer slowly-relaxing $^{13}$C coherence to $^1$H coherence that takes advantage of additional cross-correlation effects to further improve sensitivity and resolution.

$^1$H single-quantum coherences, like $^{13}$C lines, are subject to strong cross-correlated relaxation effects in $^{13}CH_2D$ groups. Interference between $^1$H–$^1$H and $^1$H–$^{13}$C dipolar interactions give rise to slowly-relaxing $^1$H coherences, $C_\beta|1\rangle\langle2|$, $C_\beta|2\rangle\langle1|$, $C_\alpha|2\rangle\langle3|$, and $C_\alpha|3\rangle\langle2|$ (relaxing at the rate $R_{2,H}^{s,CH_2D}$ defined in Figure 4), and fast-relaxing coherences, $C_\alpha|1\rangle\langle2|$, $C_\alpha|2\rangle\langle1|$, $C_\beta|2\rangle\langle3|$, and $C_\beta|3\rangle\langle2|$ (relaxing with rate $R_{2,H}^{f,CH_2D}$). For what follows it is useful to define the following operators describing fast- and

slowly-relaxing in-phase $^1$H coherences along the $x$- and $y$-axes:

$$\begin{aligned}
H_x^{slow} &= (1/\sqrt{2})(C_\alpha|3\rangle\langle 2| + C_\alpha|2\rangle\langle 3| + C_\beta|2\rangle\langle 1| + C_\beta|1\rangle\langle 2|) \\
&= (1/2)(H_{1x} + H_{2x} - 4C_zH_{1x}H_{2z} - 4C_zH_{1z}H_{2x}) \\
H_y^{slow} &= (i/\sqrt{2})(C_\alpha|3\rangle\langle 2| - C_\alpha|2\rangle\langle 3| + C_\beta|2\rangle\langle 1| - C_\beta|1\rangle\langle 2|) \\
&= (1/2)(H_{1y} + H_{2y} - 4C_zH_{1y}H_{2z} - 4C_zH_{1z}H_{2y}) \\
H_x^{fast} &= (1/\sqrt{2})(C_\alpha|2\rangle\langle 1| + C_\alpha|1\rangle\langle 2| + C_\beta|3\rangle\langle 2| + C_\beta|2\rangle\langle 3|) \\
&= (1/2)(H_{1x} + H_{2x} + 4C_zH_{1x}H_{2z} + 4C_zH_{1z}H_{2x}) \\
H_y^{fast} &= (i/\sqrt{2})(C_\alpha|2\rangle\langle 1| - C_\alpha|1\rangle\langle 2| + C_\beta|3\rangle\langle 2| - C_\beta|2\rangle\langle 3|) \\
&= (1/2)(H_{1y} + H_{2y} + 4C_zH_{1y}H_{2z} + 4C_zH_{1z}H_{2y})
\end{aligned}$$

and the following operators describing coherences that are antiphase with respect to the $^{13}$C spin:

$$\begin{aligned}
2C_zH_x^{slow} &= (1/\sqrt{2})(C_\alpha|3\rangle\langle 2| + C_\alpha|2\rangle\langle 3| - C_\beta|2\rangle\langle 1| - C_\beta|1\rangle\langle 2|) \\
&= (1/2)(2C_zH_{1x} + 2C_zH_{2x} - 2H_{1x}H_{2z} - 2H_{1z}H_{2x}) \\
2C_zH_y^{slow} &= (i/\sqrt{2})(C_\alpha|3\rangle\langle 2| - C_\alpha|2\rangle\langle 3| - C_\beta|2\rangle\langle 1| + C_\beta|1\rangle\langle 2|) \\
&= (1/2)(2C_zH_{1y} + 2C_zH_{2y} - 2H_{1y}H_{2z} - 2H_{1z}H_{2y}) \\
2C_zH_x^{fast} &= (1/\sqrt{2})(C_\alpha|2\rangle\langle 1| + C_\alpha|1\rangle\langle 2| - C_\beta|3\rangle\langle 2| - C_\beta|2\rangle\langle 3|) \\
&= (1/2)(2C_zH_{1x} + 2C_zH_{2x} + 2H_{1x}H_{2z} + 2H_{1z}H_{2x}) \\
2C_zH_y^{fast} &= (i/\sqrt{2})(C_\alpha|2\rangle\langle 1| - C_\alpha|1\rangle\langle 2| - C_\beta|3\rangle\langle 2| + C_\beta|2\rangle\langle 3|) \\
&= (1/2)(2C_zH_{1y} + 2C_zH_{2y} + 2H_{1y}H_{2z} + 2H_{1z}H_{2y})
\end{aligned}$$

The average experimental values of $R_{2,H}^{s,CH_2D}$ and $R_{2,H}^{f,CH_2D}$ measured for Ile δ1 $^{13}CH_2D$ groups in MSG (Table 1) differ by a factor of 3.7. The $^1H$–$^1H$ /$^1H$–$^{13}C$ dipolar cross-correlation effect is, thus, substantial and it is clearly desirable to exploit it in any relaxation-optimized experiment for $^{13}CH_2D$ groups.

The $^{13}CH_2D$ TROSY pulse sequence (Figure 5) is designed to optimize resolution in the $^1$H dimension by converting the $^{13}$C coherence present during $t_1$ into slowly-relaxing $^1$H coherence for detection. Remarkably, a previously known planar TOCSY mixing sequence (Mádi et al., 1997) can be used for this selective transfer. The pulse train $(\pi/2)_x$–$[\tau/2$–$(\pi)_x$–$\tau/2$–$(\pi/2)_y$–$\tau/2$–$(\pi)_x$–$\tau/2]_n$–$(\pi/2)_{-x}$, where $(\theta)_{x/y}$ denotes simultaneous $^{13}$C and $^1$H pulses of tip angle θ along the $x/y$ axis, simulates evolution under the planar mixing Hamiltonian $H = \pi J_{CH}(2H_xC_x + 2H_yC_y)$ for a time $n\tau$, subject to the condition $\tau \ll 1/J_{CH}$. This has the effect of transferring the slowly-relaxing $^{13}$C coherences, $2C_x|2\rangle\langle 2|$ and $2C_y|2\rangle\langle 2|$, to the slowly-relaxing $^1$H coherences $2C_zH_x^{slow}$ and $2C_zH_y^{slow}$, respectively, and optimal transfer is obtained with $n\tau = 1/(4\sqrt{2}J_{CH})$. For the purposes of this experiment, it is not necessary to simulate the planar mixing Hamiltonian exactly, and the desired transfer can be achieved using a single cycle of the mixing sequence with optimized delays. In the $^{13}CH_2D$ TROSY sequence, the element $(\pi/2)_x$–$\tau'$–$(\pi)_x$–$\tau'$–$(\pi/2)_y$–$\tau''$–$(\pi)_x$–$\tau''$–$(\pi/2)_{-x}$ is applied after $t_1$ to effect the transfer:

$$\begin{aligned}
&2C_y|2\rangle\langle 2|\cos(\Omega_C t_1) + 2C_x|2\rangle\langle 2|\sin(\Omega_C t_1) \\
&\rightarrow (1/2)(2C_zH_y^{slow}\cos[\Omega_C t_1] \\
&\quad + 2C_zH_x^{slow}\sin[\Omega_C t_1])(\cos^2[2\pi J_{CH}\tau']\sin[4\pi J_{CH}\tau''] \\
&\quad + \sin[4\pi J_{CH}\tau']\cos[2\pi J_{CH}\tau'']) \\
&\quad + (1/2)(2C_zH_y^{fast}\cos[\Omega_C t_1] \\
&\quad - 2C_zH_x^{fast}\sin[\Omega_C t_1])(\cos^2[2\pi J_{CH}\tau']\sin[4\pi J_{CH}\tau''] \\
&\quad - \sin[4\pi J_{CH}\tau']\cos[2\pi J_{CH}\tau'']).
\end{aligned}$$

In addition to the terms listed above, some $^1H$–$^{13}C$ multiple-quantum coherence and some residual $^{13}$C coherence are also present after the transfer, but these do not contribute to the final signal and are neglected in what follows. A maximal amount of slowly-relaxing $^1$H coherence is obtained when delays of length $\tau' = 1/(12J_{CH})$ and $\tau'' = \text{asin}(1/\sqrt{3})/(2\pi J_{CH})$ are used, in which case no fast-relaxing coherence is produced and the system is left in the state $\rho = (1/\sqrt{2})(2C_zH_y^{slow}\cos[\Omega_C t_1] + 2C_zH_x^{slow}\sin[\Omega_C t_1])$ (point *e*). Notably, because this transfer preserves the equivalent $\cos(\Omega_C t_1)$ and $\sin(\Omega_C t_1)$ pathways, the experiment's sensitivity can be increased by a factor of $\sqrt{2}$ by implementing a gradient enhanced sensitivity scheme for quadrature detection in the $^{13}$C dimension (Kay et al., 1992; Schleucher et al., 1993).

The remainder of the $^{13}CH_2D$ TROSY pulse sequence consists of a refocusing element and the $^1$H acquisition period, $t_2$. Because $^{13}$C π pulses interconvert the fast- and slowly-relaxing $^1$H coherences, $^{13}$C decoupling cannot be applied during acquisition. The slowly-relaxing $^1$H coherence has components that precess at two different frequen-

cies during $t_2$ ($C_\alpha|3\rangle\langle 2|$ at $\Omega_H - \pi J_{CH}/2$ and $C_\beta|2\rangle\langle 1|$ at $\Omega_H + \pi J_{CH}/2$) giving rise to doublets in the $^1H$ dimension, but the experiment is designed to facilitate post-acquisition manipulation of the data to yield singlets using a procedure described in Appendix A. In Appendix B we present a detailed analysis of the efficiency of this pulse scheme and show that the manipulations ensuring that slowly relaxing coherences are present during key steps in the sequence lead to a decrease in the intrinsic sensitivity of the experiment by $2\sqrt{2}$.

As an aside, it is interesting to consider the use of a planar TOCSY element for the initial $^1H$ to $^{13}C$ transfer in the pulse sequence of Figure 5. Planar TOCSY is ideally suited for the $^{13}C$-to-$^1H$ step (as described above) because it effects a selective transfer between the slowly-relaxing coherences $C_x|2\rangle\langle 2|$ and $2C_zH_x^{slow}$ (and between $C_y|2\rangle\langle 2|$ and $2C_zH_y$). However, when the $^1H$-to-$^{13}C$ transfer is considered, this selectivity is a disadvantage. Using the sequence of Figure 5, steady-state $^1H$ magnetization is converted to antiphase $^1H$ coherence, $\rho = 2C_zH_x = 2C_zH_x^{slow} + 2C_zH_x^{fast}$, and each of $2C_zH_x^{slow}$ and $2C_zH_x^{fast}$ is transformed to $C_y|2\rangle\langle 2|$ with an efficiency of 50% (so that the net transfer efficiency for the sum, $2C_zH_x^{slow} + 2C_zH_x^{fast}$, is $1/\sqrt{2}$). In contrast, the planar TOCSY element in the same context transfers only the $2C_zH_y^{slow}$ component to $C_y|2\rangle\langle 2|$, with an efficiency that is $\sqrt{2}$ higher than for $2C_zH_y^{slow} \rightarrow C_y|2\rangle\langle 2|$ in the scheme of Figure 5. Regrettably, since $2C_zH_y^{fast}$ does not contribute in this case the net efficiency becomes $1/\sqrt{2}$ less than for the approach used here, neglecting relaxation during the transfer.

HSQC, HMQC, and $^{13}CH_2D$ TROSY spectra of $^{13}CH_2D$-labeled MSG, 37 °C are shown in Figure 2bi–iii. The datasets have been acquired to account as best as possible for the dramatic difference in the average relaxation rates of operative coherences during the indirectly detected acquisition period (Table 1); thus acquisition times of 32 ms were used in $t_1$ for the HSQC and HMQC maps, while $t_1^{max} = 80$ ms was employed in the case of the TROSY. The number of transients in each experiment has been adjusted so that the net acquisition time for each spectrum is the same. In this way the average sensitivity of the HSQC experiment is not marginalized by the rapid decay of $^{13}C$ magnetization, although this fast relaxation is reflected in the resolution in $F_1$. The TROSY spectrum (Figure 2biii) shows a striking improvement in resolution over the HSQC (Figure 2bi) and HMQC (Figure 2bii) datasets. Nevertheless, there is a significant sensitivity drop (Figure 2bv) which reflects the facts that the sequence is inherently $2\sqrt{2}$ less sensitive and that $t_1^{max}$ values (and consequently the number of scans) are adjusted in each experiment to reflect the difference in $T_2$ values. For more than half of the residues that could be quantified, the ratio of the signal-to-noise in the HSQC relative to the $^{13}CH_2D$ TROSY is between 1.2 and 2.0 (i.e., less than the $2\sqrt{2}$ that would be predicted in the absence of relaxation) due to the substantially improved linewidths for the TROSY in $F_2$ (see above). For a smaller number of correlations the sensitivity is far better for the HSQC (ratios < 3); these peaks derive from residues where the 'slowly-relaxing' carbon coherence, $C_{x,y}|2\rangle\langle 2|$, decays much more rapidly than average (possibly due to exchange) or where the decay of the fast-relaxing $C_{x,y}|1\rangle\langle 1|$, $C_{x,y}|3\rangle\langle 3|$ terms is slower than average (due to ps–ns time scale motions). An analysis of the intensities of correlations for MSG, 37 °C ($\tau_c \sim 55$ ns) measured in each of the HSQC, HMQC and TROSY datasets shows average sensitivities of 1.0:0.88:0.51 (based on 24 cross peaks that are quantified in each of the datasets of Figure 2b), although it is important to emphasize that the distributions of intensities are far from Gaussian and the averages are very much skewed by outliers (Figure 2biv,v). Of interest, when the HSQC and TROSY-based experiments are modified for the measurement of $^2H$ relaxation rates in $^{13}CH_2D$ groups attached to high molecular weight proteins by including substantial additional delays during which $^{13}C$ magnetization evolves, the TROSY experiment emerges as the more sensitive by a factor of 2 (Tugarinov et al., 2005b), although there is a wide distribution in the sensitivity ratios of different residues (from 0.5 to 4.0).

### *$^{13}CHD_2$ methyl groups*

HSQC and HMQC spectra of $^{13}CHD_2$-labeled MSG at 37 °C are shown in Figure 2ci and cii, respectively. The $^{13}CHD_2$ methyl essentially comprises an AX spin system and it is therefore not surprising that both HSQC and HMQC datasets are well resolved, with correlations of similar intensities (see below).

We have also developed a $^{13}CHD_2$ HZQC pulse sequence (Figure 6), similar to the improved $^{13}CH_3$ HZQC pulse scheme (Figure 3), that provides better resolution in the indirectly detected dimension than HSQC and HMQC. The relaxation of $^1H$–$^{13}C$ multiple-quantum coherences in this spin system is dominated by intra-methyl $^{13}C$–D and $^1H$–D dipolar interactions, and cross-correlation between these interactions enhances the relaxation of double-quantum coherences while slowing the relaxation of zero-quantum elements. For an isolated $^{13}CHD_2$ spin system tumbling in the macromolecular limit, the relaxation rates for double and zero-quantum coherences are given by

$$R_{DQ}^{CHD_2} = \frac{4}{15}\left(\frac{\mu_0}{4\pi}\right)^2\frac{\gamma_H^2\gamma_D^2\hbar^2 S_{axis}^2\tau_C}{r_{HD}^6} + \frac{16}{135}\left(\frac{\mu_0}{4\pi}\right)^2\frac{\gamma_C^2\gamma_D^2\hbar^2 S_{axis}^2\tau_C}{r_{CD}^6} + \frac{16}{45}\left(\frac{\mu_0}{4\pi}\right)^2\frac{\gamma_H\gamma_C\gamma_D^2\hbar^2 S_{axis}^2\tau_C}{r_{HD}^3 r_{CD}^3} \quad \text{and}$$

$$R_{ZQ}^{CHD_2} = \frac{4}{15}\left(\frac{\mu_0}{4\pi}\right)^2\frac{\gamma_H^2\gamma_D^2\hbar^2 S_{axis}^2\tau_C}{r_{HD}^6} + \frac{16}{135}\left(\frac{\mu_0}{4\pi}\right)^2\frac{\gamma_C^2\gamma_D^2\hbar^2 S_{axis}^2\tau_C}{r_{CD}^6} - \frac{16}{45}\left(\frac{\mu_0}{4\pi}\right)^2\frac{\gamma_H\gamma_C\gamma_D^2\hbar^2 S_{axis}^2\tau_C}{r_{HD}^3 r_{CD}^3},$$

respectively, where all symbols are as described for the $^{13}CH_2D$ relaxation rates given in Figure 4 and where the same assumptions as used in that derivation (see above) have been employed. The cross-correlation contribution to $R_{ZQ}^{CHD_2}$ essentially negates the auto-correlated $^1H$–D and $^{13}C$–D dipolar contributions, and as a result, $R_{DQ}^{CHD_2}$ and $R_{ZQ}^{CHD_2}$ can differ by an order of magnitude, although this difference is reduced when relaxation contributions from dipolar interactions with spins external to the $^{13}CHD_2$ group are considered. Thus, although there is a twofold reduction in the intrinsic sensitivity of the HZQC experiment relative to the HSQC/HMQC schemes (due to the elimination of the transfer pathway involving double quantum coherence), this loss can be compensated for in applications involving high molecular weight proteins due to the reduced line widths in the indirectly detected dimension. The relative intensities of correlations measured in the HSQC, HMQC and HZQC datasets of Figure 2c are 0.93:0.96:1.0, respectively (average over 36 residues). Figure 2civ,v shows histograms of intensity ratios obtained in the various experiments.

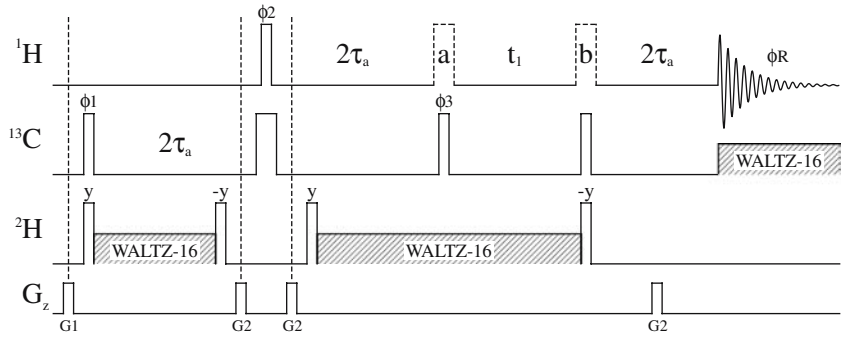


*Figure 6*. Pulse sequence for zero-quantum $^1H$–$^{13}C$ correlation spectroscopy of $^{13}CHD_2$-labeled methyl groups ($^{13}CHD_2$ HZQC). Each narrow (wide) rectangular pulse is applied along the *x*-axis with the highest available power (except for $^2H$ where a 2 kHz field is employed) and with a tip angle of $\pi/2$ ($\pi$), unless otherwise indicated. WALTZ-16 decoupling on the $^{13}C$ ($^2H$) channel is applied using a 2–3 kHz (0.75 kHz) field. For each $t_1$ point, the pulse sequence is repeated once with the $^1H$ $\pi$ pulse at position a and once with the $^1H$ $\pi$ pulse at position b (dotted lines), giving rise to two separate datasets that are subsequently added and subtracted to generate sensitivity-enhanced hypercomplex data as described previously (Cavanagh and Rance, 1993). Pulse phases are cycled as follows: $\phi2 = x, y; \phi3 = y, -x, -y, x$; when the $^1H$ $\pi$ pulse is applied at position a, $\phi1 = -y, -x, y, x$ and $\phi R = x, -x, -x, x$; and when the $^1H$ $\pi$ pulse is applied at position b, $\phi1 = y, x, -y, -x$ and $\phi R = x, x, -x, -x$. Delay $\tau_a$ is set to 1.8 ms. The (durations, strengths) of the field gradient pulses ($G_z$) are G1 = (2.0 ms, 4 G/cm) and G2 = (0.35 ms, 24 G/cm).

*Table 2.* Expressions for the relative sensitivities of several $^{13}C$–$^{1}H$ correlation experiments on $^{13}CH_nD_{3-n}$ methyl groups attached to molecules tumbling in the macromolecular limit

| Isotopomer, experiment | Relative theoretical sensitivity[a] |
|---|---|
| $^{13}CH_3$, HMQC | $S_{HMQC}^{CH_3}=\frac{3}{2}\left[\exp\left(-R_{2,H}^{s,CH_3}/J_{CH}\right)H_1\left(R_{2,CH}^{s,CH_3},t_1^{max}\right)H_1\left(R_{2,H}^{s,CH_3},t_2^{max}\right)+\exp\left(-R_{2,H}^{f,CH_3}/J_{CH}\right)H_1\left(R_{2,CH}^{f,CH_3},t_1^{max}\right)H_1\left(R_{2,H}^{f,CH_3},t_2^{max}\right)\right]\left[1-\exp\left(-R_{1,H}^{CH_3}d_1\right)\right]$ |
| $^{13}CH_2D$, HSQC | $S_{HSQC}^{CH_2D}=\frac{1}{2}\left[\exp\left(-R_{2,H}^{s,CH_2D}/2J_{CH}\right)+\exp\left(-R_{2,H}^{f,CH_2D}/2J_{CH}\right)\right]^2H_1\left(R_{2,C}^{f,CH_2D},t_1^{max}\right)\times H_2\left(\frac{1}{2}\left(R_{2,H}^{s,CH_2D}+R_{2,H}^{f,CH_2D}\right),t_2^{max},J_{HD}\right)\left[1-\exp\left(-R_{1,H}^{CH_2D}d_1\right)\right]$ |
| $^{13}CH_2D$, TROSY (Figure 5) | $S_{TROSY}^{CH_2D}=\frac{1}{4\sqrt{2}}\left[\exp\left(-R_{2,H}^{s,CH_2D}/2J_{CH}\right)+\exp\left(-R_{2,H}^{f,CH_2D}/2J_{CH}\right)\right]\exp\left(-2R_{TOCSY}^{CH_2D}(\tau'+\tau'')\right)\times\exp\left(-\left(R_{2,C}^{s,CH_2D}+R_{2,C}^{f,CH_2D}\right)/4J_{CH}\right)H_1\left(R_{2,C}^{s,CH_2D},t_1^{max}\right)\times\left[\exp\left(-R_{2,H}^{s,CH_2D}/4J_{CH}\right)+\exp\left(-R_{2,H}^{f,CH_2D}/4J_{CH}\right)\right]H_2\left(R_{2,H}^{s,CH_2D},t_2^{max},J_{HD}\right)\times\left[1-\exp\left(-R_{1,H}^{CH_2D}d_1\right)\right]$ |
| $^{13}CHD_2$, HSQC[b] | $S_{HSQC}^{CHD_2}=\exp\left(-R_{2,H}^{CHD_2}/J_{CH}\right)H_1\left(R_{2,C}^{CHD_2},t_1^{max}\right)H_3\left(R_{2,H}^{CHD_2},t_2^{max},J_{HD}\right)\left[1-\exp\left(-R_{1,H}^{CHD_2}d_1\right)\right]$ |

[a] In these expressions, $J_{CH}$ and $J_{HD}$ are coupling constants for one-bond $^{1}H$–$^{13}C$ and two-bond $^{1}H$–D couplings within the methyl group, $d_1$ is the relaxation delay between repetitions of an experiment, and $t_1^{max}$ and $t_2^{max}$ are the acquisition times in the indirectly and directly detected dimensions, respectively. Relaxation rates are written in the notation used in Table 1, except for $R_{TROSY}^{CH_2D}$, which is the effective relaxation rate during the planar TOCSY period of the $^{13}CH_2D$ TROSY experiment. The function $H_1(R, t) = [1 - \exp(-Rt)]/R$, which gives the maximum intensity of a one-dimensional Lorentzian line that includes the effect of finite acquisition time, is used to account for relaxation during $^{13}C$ chemical shift encoding periods and $^{1}H$ acquisition periods. The functions $H_2(R, t, J_{HD}) = [1-\exp(-Rt)]/3R + (2/3)\Lambda(R, t, 2\pi J_{HD})$ and $H_3(R, t, J_{HD}) = [1-\exp(-Rt)]/3R + (4/9)\Lambda(R, t, 2\pi J_{HD}) + (2/9)\Lambda(R, t, 4\pi J_{HD})$, where $J_{HD}$ is the two-bond intra-methyl $^{1}H$–$^{2}H$ coupling constant and $\Lambda(R, t, \nu) = \{\exp(-Rt)[-R\cos(\nu t) + \nu\sin(\nu t)] + R\}/(R^2 + \nu^2)$, are similar to $H_1(R, t)$ but also account for the effects of $^{1}H$–$^{2}H$ coupling during $^{1}H$ acquisition for $^{13}CH_2D$ and $^{13}CHD_2$ groups, respectively. The planar TOCSY transfer delays are defined as $\tau' = 1/(12J_{CH})$ and $\tau'' = \text{asin}(1/\sqrt{3})/(2\pi J_{CH})$.
[b] For a non-sensitivity-enhanced HSQC pulse sequence.

*Comparison of spectra recorded on the different isotopomers*

The relaxation properties of $^{13}CH_3$, $^{13}CH_2D$, and $^{13}CHD_2$ labeled methyl groups attached to macromolecules are subtle and must be considered in terms of the coherence transfer pathways generated by specific pulse sequences. Thus, although it is tempting to conclude that the transverse relaxation characteristics of $^{13}CHD_2$ methyls will be desirable relative to other methyl isotopomers because the number of $^{1}H$ dipoles contributing to relaxation has been minimized, the situation is, in general, more complex. The relaxation-optimized experiments discussed above, which partially or fully negate the effects of $^{1}H$–$^{1}H$ and $^{1}H$–$^{13}C$ interactions for all three isotopomers, allow $^{1}H$–$^{13}C$ correlation spectra of comparable resolution to be recorded for all three methyl types.

However, there are large sensitivity differences between the optimal experiments for $^{13}CH_3$, $^{13}CH_2D$ and $^{13}CHD_2$ groups. This can be appre-

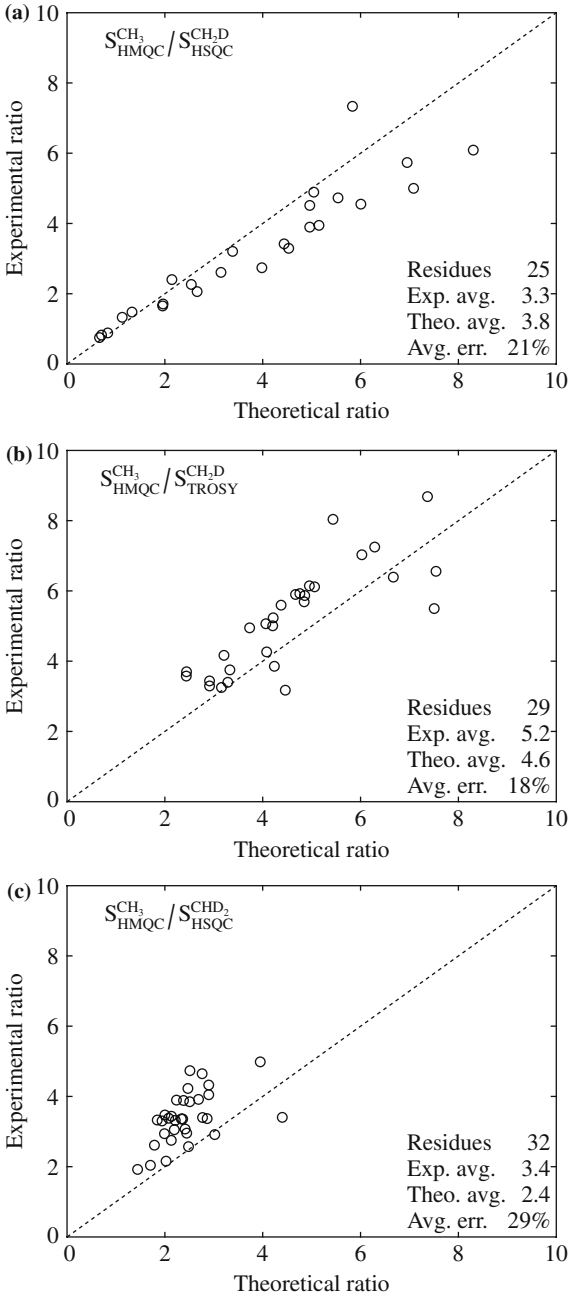


*Figure 7.* Comparison of experimentally observed to theoretically predicted ratios of sensitivity between (a) $^{13}CH_3$ HMQC vs. $^{13}CH_2D$ HSQC, (b) $^{13}CH_3$ HMQC vs. $^{13}CH_2D$ TROSY, and (c) $^{13}CH_3$ HMQC vs. $^{13}CHD_2$ HSQC (not sensitivity-enhanced) datasets recorded on appropriately labeled samples of malate synthase G. Theoretical sensitivity ratios were obtained by evaluating the expressions in Table 2 with residue-specific relaxation rates measured as described in Materials and methods. In evaluating $S^{CH_2D}_{TROSY}$ it was assumed that $R^{CH_2D}_{TOCSY} = \frac{1}{4}(R^{s,CH_2D}_{2,H} + R^{f,CH_2D}_{2,H} + R^{s,CH_2D}_{2,C} + R^{f,CH_2D}_{2,C})$. Values of $S^{CH_2D}_{HSQC}$ and $S^{CH_2D}_{HMQC}$ were adjusted to account for the fact that these spectra were recorded with different numbers of scans/FID and a different $t_1^{max}$ than the other spectra (see Materials and methods). Experimental sensitivity ratios were quantified as ratios of maximum peak intensities measured from spectra recorded as described in Materials and methods and normalized to the same noise floor. Experimental intensities from the HSQC and $^{13}CH_2D$ TROSY experiments on $^{13}CH_2D$-labeled MSG were multiplied by 1/0.9 to account for the 10% $^{13}CHD_2$ impurity present in the α-ketobutyrate precursor used to produce this sample.

ciated from a consideration of the operative coherence transfer pathways in each experiment, where the effects of relaxation are included. Table 2 lists expressions derived for these sensitivities in terms of measurable single-exponential relaxation rates. In addition, intensities of correlations can be quantified from the experiments and compared between isotopomers. Here we have measured peak intensities in the HMQC spectrum of $^{13}CH_3$-labeled MSG, the HSQC and $^{13}CH_2D$ TROSY spectra of $^{13}CH_2D$-labeled MSG and the HSQC spectrum of $^{13}CHD_2$-labeled MSG. We report relative sensitivity on a per-residue basis in terms of the ratio of peak intensities observed for a specific Ile δ1 methyl group in a test spectrum vs. a reference spectrum, where both spectra have been normalized to have the same noise floor. The HMQC spectrum of $^{13}CH_3$-labeled MSG is used as the reference. Three sets of experimental intensity ratios are shown in Figure 7, plotted against theoretical sensitivity ratios obtained using the expressions in Table 2. The HMQC dataset of $^{13}CH_3$-labeled MSG is, on average, 3.3 and 5.2 times as sensitive as the HSQC and TROSY spectra recorded on $^{13}CH_2D$-labeled MSG, respectively, and 3.4 times as sensitive as the HSQC correlation map obtained from $^{13}CHD_2$-labeled MSG (although comparison with a dataset obtained from a sensitivity-enhanced HSQC pulse sequence reduces this factor to 2.6). The results in Figure 7 also serve to validate the expressions in Table 2, as the theoretical sensitivities are reasonably consistent with experiment, with average errors of 21%, 18%, and 29% in the comparisons of Figure 7a–c, respectively.

This study clearly establishes that the $^{13}CH_3$ isotopomer is best in structural studies of proteins where methyl groups are used as probes. Using the HMQC or the $^{13}CH_3$ HZQC (Figure 3) pulse sequence, $^1H$–$^{13}C$ correlation spectra of a $^{13}CH_3$ labeled sample can be recorded with much greater

sensitivity than can be achieved using $^{13}CH_2D$ or $^{13}CHD_2$ labeling and with comparable resolution. In a pairwise comparison of the nine spectra of Figure 2, the average ratio of intensities between corresponding peaks in the $^{13}CH_3$ HMQC (Figure 2aii) and the $^{13}CHD_2$ HZQC (Figure 2ciii) spectra is 2.4, with larger ratios obtained when the $^{13}CH_3$ HMQC is compared to other datasets. The sensitivity advantage arises because the $^{13}CH_3$ isotopomer has the largest number of $^1H$ spins contributing polarization to the signal and because fast and slowly relaxing components are isolated automatically without additional elements such as those used in the $^{13}CH_2D$ TROSY sequence. In addition, recovery of equilibrium $^1H$ magnetization is relatively fast for $^{13}CH_3$ methyls, a factor which accounts for approximately half of the sensitivity difference between $^{13}CH_3$ HMQC and experiments on $^{13}CHD_2$ labeled groups. Finally, it is important to note that, while $^{13}CH_3$ labeling is best for many purposes, the ability to produce samples that are uniformly labeled with $^{13}CH_2D$ or $^{13}CHD_2$ facilitates studies of side chain dynamics via $^2H$ spin relaxation (Tugarinov et al., 2005b) and allows a rigorous 'dissection' of relaxation in methyl spin systems through comparison of results obtained on the different isotopomers.

**Acknowledgements**

This work was supported by a grant from the Canadian Institutes of Health Research to L.E.K., who also holds a Canada Research Chair in Biochemistry. J.O. and V.T. acknowledge the support of the Natural Sciences and Engineering Research Council of Canada and the Human Frontiers Science Program, respectively.

## Appendix A: Post-acquisition removal of $^1H$-$^{13}C$ scalar coupling derived splittings from the $^1H$ dimension of the $^{13}CH_2D$ TROSY spectrum

When the pulse sequence of Figure 5 is applied to a $^{13}CH_2D$ spin system attached to a macromolecule, the system's state at point *e* in the scheme is

$$\rho = (1/\sqrt{2})(2C_zH_y^{slow}\cos[\Omega_C t_1] + 2C_zH_x^{slow}\sin[\Omega_C t_1]).$$

Contributions to the final signal deriving from the $\cos(\Omega_C t_1)$ and $\sin(\Omega_C t_1)$ components of this density matrix are separated and recombined post-acquisition as part of a gradient enhanced sensitivity scheme (Kay et al., 1992; Schleucher et al., 1993). For simplicity, in the following discussion we will consider only the $\cos(\Omega_C t_1)$ component by setting $t_1 = 0$, and state without further proof that the behavior of the $\sin(\Omega_C t_1)$ component is similar. This simplifies the density matrix to

$$\rho = (1/\sqrt{2})2C_zH_y^{slow}.$$

The remainder of the experiment consists of a refocusing element and the $^1H$ acquisition period, $t_2$. During the refocusing period, the system is allowed to evolve under $^1H$–$^{13}C$ scalar coupling for a duration of $\tau_b = 1/(4J_{CH})$, so that an equal superposition of in-phase and antiphase coherences is present at the beginning of $t_2$.

Two datasets are recorded using slightly different versions of the pulse sequence. In one version, a $^{13}C$ $\pi$ pulse is applied immediately before acquisition, so that $\rho = -(1/2)(2C_zH_y^{slow} + H_x^{slow})$ at the beginning of $t_2$ (this corresponds to $\phi_5 = \phi_6 = x$ in Figure 5). Let us refer to the resulting dataset as[2]

$$S_1 = S(2C_zH_y^{slow} + H_x^{slow}).$$

In the second version of the experiment, the final $^{13}C$ $\pi$ pulse is removed and the phase of the $\pi/2$ $^{13}C$ pulse preceding the refocusing period is inverted, so that $\rho = -(1/2)(2C_zH_y^{slow} - H_x^{slow})$ at the beginning of acquisition ($\phi_5 = \phi_6 = -x$ in Figure 5; the $\pi$ pulse is effectively replaced by a pulse of the same duration with no net effect). This experiment yields the dataset

$$S_2 = S(2C_zH_y^{slow} - H_x^{slow}).$$

Taking the sum and difference of $S_1$ and $S_2$ isolates the antiphase and in-phase components of the signal in two new datasets, $S_3$ and $S_4$:

$$S_3 = S_1 + S_2 = S(2C_zH_y^{slow})$$
$$S_4 = S_1 - S_2 = S(H_x^{slow})$$

[2] The notation $S(\rho)$ represents the data set that is obtained when the system is in state $\rho$ at the beginning of the $^1H$ acquisition period. Because acquisition is a linear operation, combining two datasets post-acquisition is analogous to combining the corresponding density matrices before acquisition; i.e. $S(\rho_1) + S(\rho_2) = S(\rho_1 + \rho_2)$.

Dataset $S_3$ is subjected to a $\pi/2$ phase shift in the $^1$H dimension to give $S_5$:

$$S_3 \rightarrow \text{ phase shift} \rightarrow S_5 = S(2C_zH_x^{slow})$$

Taking the sum and difference of $S_4$ and $S_5$ isolates the upfield and downfield components of the $^1$H doublets in two new datasets, $S_6$ and $S_7$:

$$S_6 = S_4 + S_5 = S([I/2 + C_z]H_x^{slow})$$
(upfield doublet components)
$$S_7 = S_4 - S_5 = S([I/2 - C_z]H_x^{slow})$$
(downfield doublet components)

A downfield (upfield) $J_{CH}/2$ frequency shift in the $^1$H dimension is applied to dataset $S_6$ ($S_7$), relying on the fact that $^1J_{CH}$ values are very uniform in Ile methyl groups. Finally, the frequency-shifted data sets are combined and processed to yield a single spectrum with the desired singlets in the $^1$H dimension.

It should be noted that, when relaxation effects are ignored, this procedure is a factor of $\sqrt{2}$ less efficient than conventional decoupling. When $^{13}$C decoupling is applied during acquisition, the upfield and downfield components of the $^1$H signal combine to form a single signal with twice the intensity. When the $^1$H doublets are instead collapsed using the post-acquisition method described here, noise collected at the frequencies of the upfield and downfield peaks is combined in the final spectrum, so that the net increase in the signal-to-noise ratio is only a factor of $\sqrt{2}$. However, as noted in the main text, the effective relaxation rate of the $^1$H coherence observed in this experiment increases dramatically when $^{13}$C decoupling is applied and relaxation-related gains in sensitivity and resolution obtained in the absence of $^{13}$C decoupling more than compensate for the lost factor of $\sqrt{2}$ discussed here.

## Appendix B: Inherent sensitivity of the $^{13}CH_2D$ TROSY experiment

When applied to a $^{13}CH_2D$ spin system, the $^{13}CH_2D$ TROSY pulse sequence (Figure 5) is inherently less sensitive by a factor of $2\sqrt{2}$ than HSQC or HMQC, in the absence of relaxation. This factor, which reflects the cost of selecting for slowly-relaxing coherences in the TROSY sequence, is the product of three independent contributions which each reduce the sequence's sensitivity by $\sqrt{2}$. In the following, these three contributions will be explained in detail, beginning with a discussion of how the efficiency of a coherence transfer element can be quantified.

The density matrix $\rho$, when expanded over an orthogonal set of product operators $\{\mathbf{B}_k\}$ normalized such that $\mathrm{Tr}\{\mathbf{B}_n\mathbf{B}_m\} = \delta_{nm}$, can be interpreted as a vector in Liouville space, $\rho = \sum_k b_k\mathbf{B}_k$. Based on the work of Sorensen (1989), the efficiency, $E$, of a transfer step in an NMR experiment can be measured in terms of the norm of this vector: $E = \|\rho_f\|/\|\rho_i\|$, where $\|\rho\| = \sqrt{(\sum_k b_k^2)}$, $\rho_i$ and $\rho_f$ represent the density matrix before and after the transfer, respectively, and terms in $\rho_i$ and $\rho_f$ that do not lie on a coherence transfer pathway leading to detectable magnetization at the end of the experiment are neglected.

This formalism will be now used to establish that a factor of $\sqrt{2}$ in inherent sensitivity is lost during each of two transfer steps in the $^{13}CH_2D$ TROSY pulse sequence. First, a transfer element involving a $^1$H mixing pulse is used to convert fast-relaxing to slowly-relaxing $^{13}$C coherence before $t_1$. Before the $^1$H pulse (at point $b$ in Figure 5), the state of the spin system is $\rho_i = -\sqrt{2}(\sqrt{2}C_z|1\rangle\langle 1| + \sqrt{2}C_z|3\rangle\langle 3|)$, and after the pulse the state is $\rho_f = -\sqrt{2}(\sqrt{2}C_z|2\rangle\langle 2|)$ (neglecting terms that do not eventually lead to detectable magnetization). The operators $\sqrt{2}C_z|n\rangle\langle n|$ ($n = 1,2,3$) are orthonormal, so the efficiency of the transfer is $E = \|\rho_f\|/\|\rho_i\| = \sqrt{2}/2 = 1/\sqrt{2}$. Later in the sequence, a planar TOCSY element is used to transfer slowly-relaxing $^{13}$C coherence present at the end of $t_1$ ($\rho_i$) to slowly-relaxing $^1$H coherence ($\rho_f$). Without loss of generality, we can consider the $t_1 = 0$ case so that $\rho_i = \sqrt{2}(\sqrt{2}C_y|2\rangle\langle 2|)$. Neglecting relaxation during the transfer and dropping terms that do not lead to detectable magnetization, $\rho_f = 1(\sqrt{2}C_zH_y^{slow})$ (point $e$ in Figure 5). It is readily established that $\sqrt{2}C_y|2\rangle\langle 2|$ and $\sqrt{2}C_zH_y^{slow}$ are mutually orthonormal. Therefore, the efficiency of this transfer is $E = \|\rho_f\|/\|\rho_i\| = 1/\sqrt{2}$.

In the calculation above the transfer efficiency from slowly relaxing carbon to slowly relaxing proton elements has been ascertained, but what is detected in the NMR experiment is not $H_x^{slow}$ but rather $H_x$. The inherent sensitivity of the experiment is thus further reduced (by a third factor of

$\sqrt{2}$, see below) because the slowly-relaxing coherence present during the $^1$H acquisition period, $t_2$, gives rise to a less intense signal than would ordinary $^1$H coherence. This can be understood by noting that $H_x^{slow} = (1/2)(H_{1x} + H_{2x} - 4C_zH_{1x}H_{2z} - 4C_zH_{1z}H_{2x})$ has components $4C_zH_{1x}H_{2z}$ and $4C_zH_{1z}H_{2x}$ that do not contribute to the detected signal (see text). The signal observed in a $^1$H-detected experiment is given by $I = \mathrm{Tr}\{\rho \cdot M\}$, where $\rho$ is the system's density matrix during acquisition and M is the normalized observable operator. In the $^{13}CH_2D$ TROSY experiment, for the purpose of this discussion we can assume that the density matrix is proportional to $H_x^{slow}$ at the beginning of $t_2$. If the observable operator were $M = (1/\sqrt{2})H_x^{slow}$ (the normalized form of $H_x^{slow}$), the initial intensity of the signal would be $I = \mathrm{Tr}\{H_x^{slow} \cdot M\} = \sqrt{2}$. However, as indicated above, the observable operator is actually $M = (1/2)H_x$ (the normalized form of $H_x = H_{1x} + H_{2x} = H_x^{slow} + H_x^{fast}$), so the initial signal intensity is $I = \mathrm{Tr}\{H_x^{slow} \cdot M\} = 1$. The observed signal is therefore a factor of $\sqrt{2}$ less than it would be if all components of $H_x^{slow}$ were detectable.

As an aside, the inherent sensitivity of $^{13}CH_2D$ TROSY is affected by two other considerations in addition to the factors discussed above. First, a sensitivity loss of $\sqrt{2}$ is associated with the post-acquisition removal of $J_{HC}$ splittings in the $^1$H dimension, as discussed in Appendix A. Also, because the planar TOCSY transfer from $^{13}$C to $^1$H preserves both sine- and cosine-modulated $t_1$ components, a gradient enhanced sensitivity scheme can be used to increase sensitivity by a factor of $\sqrt{2}$. Thus, when taken together these two issues have no net effect.

## References


Bax, A., Griffey, R.H. and Hawkins, B.L. (1983) *J. Magn. Reson.*, **55**, 301–315.

Bodenhausen, G. and Rubin, D.J. (1980) *Chem. Phys. Lett.*, **69**, 185–189.

Delaglio, F., Grzesiek, S., Vuister, G.W., Zhu, G., Pfeifer, J. and Bax, A. (1995) *J.Biomol. NMR*, **6**, 277–293.

Gardner, K.H. and Kay, L.E. (1997) *J. Am. Chem. Soc.*, **119**, 7599–7600.

Gardner, K.H., Rosen, M.K. and Kay, L.E. (1997) *Biochemistry*, **36**, 1389–1401.

Goto, N.K., Gardner, K.H., Mueller, G.A., Willis, R.C. and Kay, L.E. (1999) *J. Biomol. NMR*, **13**, 369–374.

Ishima, R., Louis, J.M. and Torchia, D.A. (1999) *J. Am. Chem. Soc.*, **121**, 11589–11590.

Ishima, R., Petkova, A.P., Louis, J.M. and Torchia, D.A. (2001) *J. Am. Chem. Soc.*, **123**, 6164–6171.

Janin, J., Miller, S. and Chothia, C. (1988) *J. Mol. Biol.*, **204**, 155–164.

Kay, L.E., Keifer, P. and Saarinen, T. (1992) *J. Am. Chem. Soc.*, **114**, 10663–10665.

Kay, L.E. and Prestegard, J.H. (1987) *J.Am. Chem. Soc.*, **109**, 3829–3835.

Kay, L.E. and Torchia, D.A. (1991) *J. Magn. Reson.*, **95**, 536–547.

Korzhnev, D.M., Kloiber, K. and Kay, L.E. (2004) *J. Am. Chem. Soc.*, **126**, 7320–7329.

Mádi, Z.L., Brutscher, B., Schulte-Herbrüggen, T., Brüschweiler, R. and Ernst, R.R. (1997) *Chem. Phys. Lett.*, **268**, 300–305.

Metzler, W.J., Wittekind, M., Goldfarb, V., Mueller, L. and Farmer, B.T. (1996) *J. Am. Chem. Soc.*, **118**, 6800–6801.

Miclet, E., Williams, D.C., Clore, G.M., Bryce, D.L., Boisbouvier, J. and Bax, A. (2004) *J. Am. Chem. Soc.*, **126**, 10560–10570.

Millet, O., Muhandiram, D.R., Skrynnikov, N.R. and Kay, L.E. (2002) *J. Am. Chem. Soc.*, **124**, 6439–6448.

Muhandiram, D.R., Yamazaki, T., Sykes, B.D. and Kay, L.E. (1995) *J. Am. Chem. Soc.*, **117**, 11536–11544.

Müller, L. (1979) *J. Am. Chem. Soc.*, **101**, 4481–4484.

Muller, N., Bodenhausen, G. and Ernst, R.R. (1987) *J. Magn. Reson.*, **75**, 297–334.

Ollerenshaw, J.E., Tugarinov, V. and Kay, L.E. (2003) *Magn. Reson. Chem.*, **41**, 843–852.

Pervushin, K., Riek, R., Wider, G. and Wuthrich, K. (1997) *Proc.Natl. Acad. Sci. USA*, **94**, 12366–12371.

Rosen, M.K., Gardner, K.H., Willis, R.C., Parris, W.E., Pawson, T. and Kay, L.E. (1996) *J. Mol. Biol.*, **263**, 627–636.

Schleucher, J., Sattler, M. and Griesinger, C. (1993) *Angew. Chem. Int. Ed. Engl.*, **32**, 1489–1491.

Shaka, A.J., Keeler, J., Frenkiel, T. and Freeman, R. (1983) *J. Magn. Reson.*, **52**, 335–338.

Smith, B.O., Ito, Y., Raine, A., Teichmann, S., Bentovim, L., Nietlispach, D., Broadhurst, R.W., Terada, T., Kelly, M., Oschkinat, H., Shibata, T., Yokoyama, S. and Laue, E.D. (1996) *J. Biomol. NMR*, **8**, 360–368.

Sørensen, O.W. (1989) *Prog. NMR Spectrosc.*, **21**, 503–569.

Tugarinov, V., Choy, W.Y., Orekhov, V.Y. and Kay, L.E. (2005a) *Proc. Natl. Acad. Sci. USA*, **102**, 622–627.

Tugarinov, V., Hwang, P.M. and Kay, L.E. (2004a) *Annu. Rev. Biochem.*, **73**, 107–146.

Tugarinov, V., Hwang, P.M., Ollerenshaw, J.E. and Kay, L.E. (2003) *J. Am. Chem. Soc.*, **125**, 10420–10428.

Tugarinov, V. and Kay, L.E. (2004a) *J. Biomol. NMR*, **29**, 369–376.

Tugarinov, V. and Kay, L.E. (2004b) *J. Biomol. NMR,*, **28**, 165–172.

Tugarinov, V., Ollerenshaw, J.E. and Kay, L.E. (2005b) *J. Am. Chem. Soc.*, **127**, 8214–8225.

Tugarinov, V., Sprangers, R. and Kay, L.E. (2004b) *J. Am. Chem. Soc.*, **126**, 4921–4925.

Werbelow, L.G. and Marshall, A.G. (1973) *J. Magn. Reson.*, **11**, 299–313.